Departure from the Vogel behaviour in the glass transition—thermally stimulated recovery, creep and dynamic mechanical analysis studies

N.M. Alves[a], J.F. Mano[a,*], J.L. Gómez Ribelles[b], J.A. Gómez Tejedor[c]

[a]*Department of Polymer Engineering, Campus of Azurém, University of Minho, 4800-058 Guimarães, Portugal*
[b]*Center for Biomaterials and Department of Applied Thermodynamics, Universidad Politécnica de Valencia, P.O. Box 22012, E-46071 Valencia, Spain*
[c]*Center for Biomaterials and Department of Applied Physics, Universidad Politécnica de Valencia, Escuela Universitaria de Informática, E-46022 Valencia, Spain*

Abstract

In this work the study of the dynamics of the segmental motions close to T_g of a poly(methyl methacrylate), PMMA, network was analysed by distinct mechanical spectroscopy techniques. Three techniques were employed: dynamic mechanical analysis (DMA), creep and thermally stimulated recovery (TSR). The time–temperature superposition principle was applied to the DMA and creep results, and master curves were successfully constructed. A change from a Vogel to an Arrhenius behaviour was observed in these results. Above T_g it was found a distinct temperature dependence for the retardation times calculated from creep and the relaxation times calculated from DMA. This unexpected behaviour was attributed to the merging of the α and the β relaxations that occurs in PMMA systems. The apparent activation energies (E_a) were also calculated from DMA, creep and TSR experiments. Above T_g the E_a values obtained agreed very well for all the techniques. In addition, the fragility exhibited by this material was investigated by the mechanical spectroscopy techniques referred above and by differential scanning calorimetry (DSC). The obtained values of the fragility index m indicated that the PMMA network is a kinetically fragile system. The thermodynamic manifestation of the fragility was also analysed.
© 2003 Published by Elsevier Ltd.

Keywords: Poly(methyl methacrylate); Mechanical behaviour; Fragility

1. Introduction

Many liquids (including covalent, ionic and metallic) are able to solidify into a disordered glassy structure upon cooling below their melting point, if crystallisation is prevented [1–3]. The glass transition corresponds to the freezing of the liquid-like mobility at the length scale of several molecular units. Microscopically, no structural change occurs during this process, and the glass maintains the same liquid-like structure [2,3]. In a more practical point of view, the glass transition is also associated to marked changes in thermodynamic derivatives properties, such as heat capacity and thermal expansivity, at temperatures around the glass transition temperature, T_g. However, the glass transition observed in the laboratory is not a true thermodynamic phase transition because it is related to a

change from an equilibrium liquid state to a non-equilibrium glassy state. Instead, it can be seen as a kinetic event, which depends upon the crossing of an experimental time scale and the time scales for the molecular rearrangements. The glassy state is unstable because a glass is continually relaxing towards equilibrium. We could consider the glass mechanically stable for practical purposes, if experimental observations are made on time scales fast compared to the molecular motions that allow the glass to relax, though it is out of thermodynamic equilibrium. The complex features of the glass transition [4] make it one of the most difficult and unsolved problems in solid state physics and much attention has been devoted in looking for adequate manners of highlighting the universal features of glass-forming systems. The fragility concept is one of the attempts to systematise this issue, first introduced by Angell [5]. It is a measure of the rate at which the structural characteristic times, τ (or related properties, such as the shear viscosity η) decreases with increasing temperature around T_g when plotted on a normalised T_g/T plot. Here, the

* Corresponding author. Address: Department de Engenharia de Polimeros, Campus de Azurein, Universidade do Minho, 4710-057 Braga, Portugal. Tel.: +351-253-510-245; fax: +351-253-510-249.
E-mail address: jmano@dep.uminho.pt (J.F. Mano).

glass transition temperature is often defined either as the temperature at which $\tau \sim 100$ s or $\eta \sim 10^{12}$ Pa s. Such $\log \tau$ (or $\log \eta$) vs. T_g/T plots were first used by Odekop, Laughlin and Uhlmann [6,7] for small molecular glass-formers and later were popularised by Angell, who used them to correlate with transport properties of glass-formers [5]. The dynamic fragility has been related with the non-exponentiality of the structural relaxation function [8–10], the chemical structure of polymers [10,11], the structural recovery in the glassy state and the vibrational motions [10]. The terms 'strong' and 'fragile' are now familiar terms in this context. Strong liquids are those characterised by follow a near Arrhenius transport behaviour, $\tau = \tau_0 \exp(E_a/RT)$, and tend to be of tetrahedral network structure. On the other hand, ionic or van der Waals liquids are usually fragile, and connoted to the sensitivity to temperature of their structure. Here, the Angell plots present a large curvature, being the apparent activation energy at lower temperatures (near T_g) usually high (sometimes higher than the vaporisation energy). Thermodynamically, strong liquids show small ΔC_p (difference of heat capacity between liquid and glass). This difference is much higher in fragile liquids.

For an understanding of the vitrification process the strong–fragile classification has been proven to be relevant. It provides the basis for the interpretation of vitrification in terms of fundamental thermodynamic quantities from which other material properties can be predicted. However, the molecular origin of fragility is far to be completely understood. A major problem impeding progress is the way of quantifying the fragility, which has often found to depend upon the technique used for a given material [12] (e.g. dielectric, calorimetric, shear compliance, shear and tensile moduli and quasielastic light scattering experiments). The aim of this work is to analyse the influence of the mechanical spectroscopy technique employed in the study of the dynamics of segmental motions close to T_g. Three techniques will be employed in this work: (i) dynamic mechanical analysis (DMA), (ii) isothermal creep experiments and (iii) thermally stimulated creep recovery, or simply thermally stimulated recovery (TSR). In fact, one should distinguish between TSR, where the release of strain is monitored against temperature, and thermally stimulated creep, where the strain of a sample subjected to a constant load is read during heating. Both kinds of experiments were discussed in a previous work [13].

The TSR technique and its electrical equivalent technique thermally stimulated depolarisation currents (TSDC), where a static electric field is applied instead of a stress and the polarisation is monitored instead of the strain, have been used for more than 20 years [14–18]. TSR has been shown to be a very sensitive technique in polymer systems, including composites, semicrystalline polymers, inter-penetrated polymer networks and thermosets, especially if combined with DMA [13,19–23]. By means of the thermal sampling procedure (TS), the TSR technique also offers the possibility of experimentally decompose a complex process,

characterised by a distribution of characteristic times, into its quasi-individual components. This procedure enables the analysis of the fine structure of the TSR global spectra.

The relatively low equivalent frequency of TSR ($\sim 10^{-3}$–10^{-2} Hz [24]), compared with typical DMA experiments, warrants a good sensitivity on studying complex relaxation phenomena. As the time scales associated to TSR measurements are similar to those used in the description of fragility ($\tau \sim 100$ s), this technique may be directly applied in such analysis. It should be also pointed out that TSDC was already used in the particular issue of quantifying the fragility, both in low molecular weight or polymeric materials [25,26].

In this work, the glass transition dynamics studied by DMA, creep and TSR will be compared for a poly(methyl methacrylate) network. Additionally, differential scanning calorimetry (DSC) was also used in samples with different thermal histories to obtain further information about the fragility exhibited by this material.

2. Experimental section

2.1. Material

The studied material was a copolymer of methyl methacrylate (Aldrich, 99% pure) and ethylene glycol dimethacrylate (Aldrich, 98% pure) containing 5% of the latter. The polymer network was synthesised by free radical addition polymerisation using as photoinitiator 0.13% by weight of benzoin (Scharlau, 98% pure). The sample was synthesised between two glass plates to form a sheet of approximately 0.5 mm thick. The reason to work with a polymer network is to prevent permanent flow above T_g, allowing to perform both DMA, creep and TSR experiments across the glass-transition. The monomer, crosslinking agent and initiator were used as received without further purification. Polymerisation took place at room temperature for 24 h under UV radiation. The low molecular weight substances remaining in the sample after polymerisation were extracted with boiling ethanol for 24 h and then dried *in vacuo* at 70 °C for several weeks until the weight remained constant. Finally the sample was dried *in vacuo* at 180 °C for 1 h in order to eliminate possible residues that still remained in the sample.

2.2. Techniques

The DMA was performed with a Seiko DMS210 equipment in the extension mode, in isothermal conditions, at different temperatures, from 109.6 to 156.4 °C every 2 °C. At each temperature the frequency was scanned from 0.01 to 20 Hz.

Creep experiments were made with a Seiko TMA/6000 equipment in the extension mode. The maximum deformation of the sample was 1%. The stress was applied within

less than 10 s before time 0 and then maintained constant for a time between 36 and 112 min in isothermal conditions. The sample length was measured as a function of time at equal time intervals in logarithmic scale, and then, the creep compliance $D(t)$ was calculated. After creep, the stress was removed, and the sample recovered for a time twice the creep time. The experiment has been carried out at different temperatures, from 122.9 to 150.5 °C every 1 °C.

TSR experiments were carried out in a DMA7e Perkin–Elmer analyser with controlled cooling accessory in the extension mode. Continuous flux of high purity helium (flow rate of ~ 28 cm^3 min^{-1}) was used to improve heat transfer throughout the sample surroundings during the experiments.

At least two kinds of experiments can be performed with the TSR technique: the TSR global and the thermal sampling (or windowing) experiments—TS. In both types of experiments a static stress, σ_0, is applied during an isothermal period, τ_σ at a creep temperature T_σ, and during a temperature program at constant rate between T_σ and $T_\sigma - \Delta T_w$. Without any stress the strain is then partially recovered during an isothermal period at $T_\sigma - \Delta T_w$, followed by a cooling down to T_0. Finally, the strain is measured, as a function of temperature, during a heating at constant rate up to a temperature well above T_σ. The difference between both experiments is that, in a TSR global experiment $T_\sigma - \Delta T_w = T_0$, whereas in a TS experiment $\Delta T_w \sim 3$ °C and $T_0 \ll T_\sigma$. In all the experiments carried out in this work we used a heating rate of 4 °C min^{-1} and for the TS experiments $\Delta T_w = 3$ °C. More details about these tests, including more experimental details can be found elsewhere [13,22]. As discussed in a previous work [13], in some cases it is necessary to perform experiments with the same experimental parameters of the TS experiments under study but without the application of a stress in order to eliminate the thermal dilatation component. In this case this procedure was found to be negligible.

In TS experiments the recovery measured during the heating scan is due to the molecular groups that were activated during the application of a static stress σ_0, which are those having retardation times at T_σ around a certain characteristic time τ_σ which depends on the period of time in which the charge is applied. Thus, the TS experiment allows resolving the complex retardation times spectrum in nearly elementary mechanisms. On the contrary, in the TSR global experiments the complex nature of the relaxation is studied because all the conformational motions with relaxation times around τ_σ between T_σ and T_0 are activated. The ensemble of the TS experiments within the glass transition region gives an overall picture of the processes associated to the relaxation as probed at low frequencies.

The DSC experiments were carried out in a Perkin–Elmer DSC7 differential scanning calorimeter with controlled cooling accessory. The temperature of the equipment was calibrated with indium and lead standards and for the heat flow calibration only the same indium sample was used.

All calibrations were carried out during heating, at 10 °C min^{-1}. A single 10.295 mg polymer sample, sealed in an aluminium pan, was used for all DSC experiments. The DSC experiments were conducted as following: (i) the sample was heated to above $T_g = 121.4$ °C in order to erase any thermal history; (ii) the sample is then cooled to 50 °C at different scanning rates, $q_c = \mathrm{d}T/\mathrm{d}t$ (between 0.5 and 40 °C min^{-1}); (iii) data is subsequently collected during an heating ramp at 10 °C min^{-1} up to 180 °C.

3. Results and discussion

3.1. DMA and creep data

Isothermal frequency DMA scans around T_g are shown in Fig. 1(a) (storage modulus, E') and Fig. 1(b) (loss factor, tan δ). The data were obtained in the frequency window from 0.01 to 20 Hz, corresponding to times between 0.008 and 16 s. The creep compliance $D(t)$ at several temperatures is shown in Fig. 2. In this case the data were obtained in a much longer time window than the DMA data (approximately between 1 and 10^4 s).

It is still under discussion if a time–temperature superposition principle [27] is accurately fulfilled by any of these series of results. In fact the viscoelastic spectrum consists of several viscoelastic mechanisms that have different shift factors [28,29] i.e. the response of a system is thermorheologically complex. This would mean that, as Plazek and co-workers argued [30], the application of this principle to
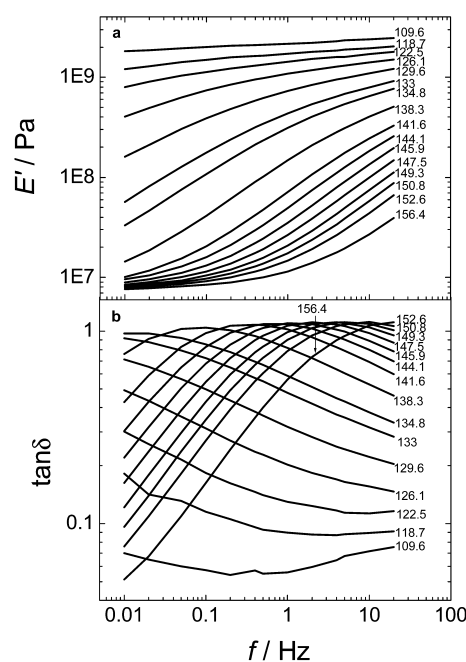

Fig. 1. DMA isothermal curves on the studied PMMA at different temperatures (in the graphics). (a) Storage modulus (E') vs. frequency. (b) Loss factor (tan δ) vs. frequency. For clarity, not all measured curves are presented.
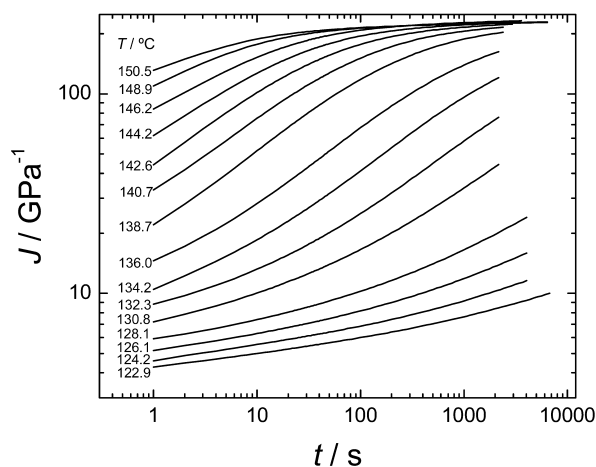
Fig. 2. Creep isothermal curves on the studied PMMA at different temperatures (in the graphics). For clarity, only an isothermal every 2 °C has been plotted.

viscoelastic data corresponding to a limited time/frequency range is possible, but it fails when it is applied for isothermal data obtained over a very broad range. In addition, the construction of master curves for PMMA could be not so straightforward because of the overlapping existing between the α and β-processes [31], even in a crosslinked material, being the β-process especially broad.

In our work, master curves for the storage modulus (E') and loss factor (tan δ) were successfully obtained by simple shifting of the isothermal results along the frequency scale, according to the time–temperature superposition principle.

Fig. 3 shows the plots of E' and tan δ as a function of reduced frequency $f a_T$, for the reference temperature $T_{ref} = 147.5$ °C.

Also, a master curve for creep compliance was constructed (Fig. 4), as a function of time, for the reference temperature $T_{ref} = 136.0$ °C. As for the case of DMA results, the master curve was obtained by simple shifting of the isothermal results along the log time scale. It should be

Fig. 4. Master curve for creep compliance obtained from horizontal displacements of the curves of Fig. 2, for a reference temperature of 136.0 °C.

pointed that in Figs. 3 and 4 all measured data were employed.

In principle, in order to account for the change in polymer density between T and T_{ref}, a vertical shift $\rho T / \rho_{ref} T_{ref}$ should be also applied to each curve of Fig. 3 and 4 [27]. However, in the studied cases this correction seemed to be negligible.

The shift factors log a_T,

$$\log a_T = \frac{\tau(T)}{\tau(T_{ref})} \tag{1}$$

for both techniques, are represented in Fig. 5 against temperature. For the DMA master curves these shift factors associated with the two curves were found to be the same. $\tau(T)$ is a relaxation time τ_E in the case of DMA results and a retardation time τ_D in the case of creep experiments. The relationship between τ_E and τ_D comes from the relationship existing between modulus, $E(t)$, and compliance, $D(t)$, in the
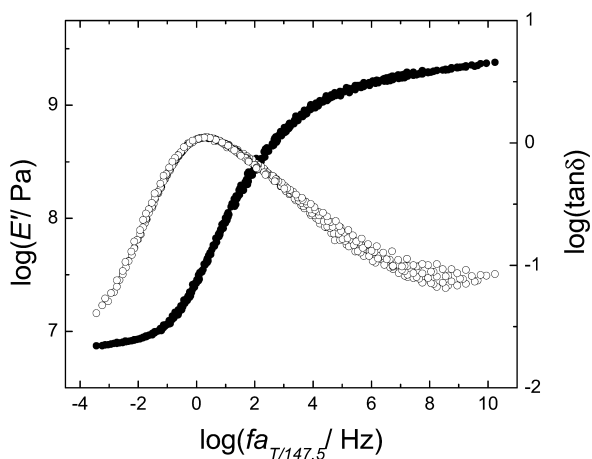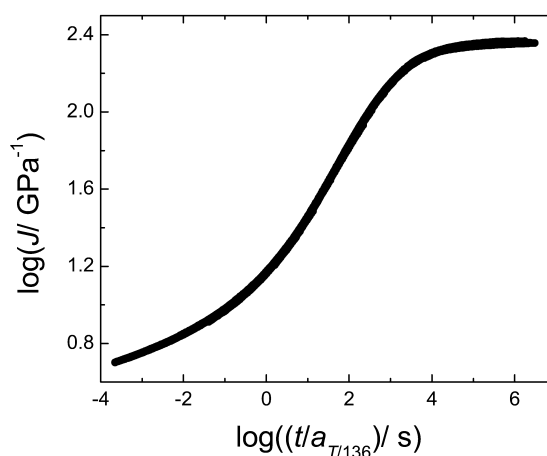

Fig. 3. Master curves for storage modulus (filled circles) and for loss factor (open circles) obtained from horizontal displacements of the curves of Fig. 1, for a reference temperature of 147.5 °C.
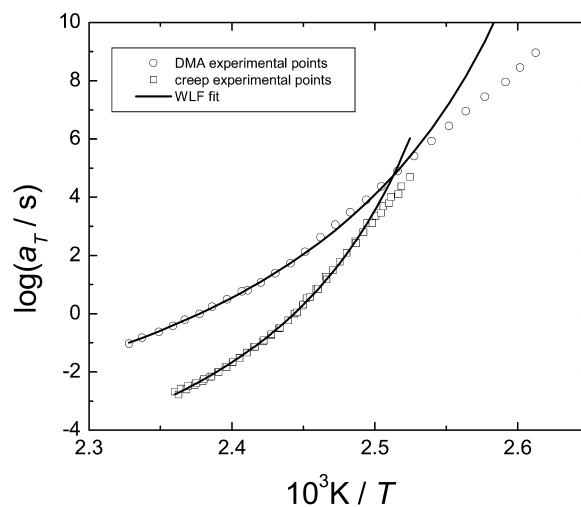

Fig. 5. Temperature dependence of the shift factors for the DMA and creep master curves presented in Figs. 3 and 4. The high temperature ranges of the data were fitted according to the WLF equation.

linear viscoelastic regime

$$\int_0^t D(t')E(t - t')dt' = t \tag{2}$$

For the case of a single relaxation time model it can be easily shown that τ_D is more than three decades longer than τ_E. If a distribution of relaxation times is considered, the difference between the times that characterise the position of the distribution in the time axis in creep and stress relaxation processes are not so high but still differences are very important. This problem will be analysed in detail elsewhere. In this work we will make use only of the derivatives of the logarithm of the relaxation times with reciprocal of temperature and, as a consequence, the absolute values of the relaxation times are not relevant for our discussion.

The shift factors above T_g, were successfully described by the WLF equation [32]

$$\log a_T = -\frac{C_1(T - T_{ref})}{C_2 + (T - T_{ref})} \tag{3}$$

where C_1 and C_2 depend on the material and on T_{ref}. This expression is usually valid for polymers over the temperature range $T_g < T < T_g + 100\,°C$ (where T_g is the glass transition temperature). Eq. (3) is equivalent to the Vogel–Fulcher–Tamman–Hesse equation (VFTH) [33–35],

$$\tau(T) = \tau_0 \exp\frac{B}{T - T_0}, \quad T_0 < T_g \tag{4}$$

where τ_0 is a pre-exponential factor and B and T_0 are specific adjustable parameters. In the VFTH equation T_0 is a diverging temperature, implying the physical impossibility of configurational changes in the solid (the configurational entropy, S_c, tends to 0 at that temperature), close to the so-called Kauzmann temperature and B/T_0 is a parameter which can be related with the fragility exhibited by the material: $B/T_0 > 30$ represents a strong behaviour and $B/T_0 < 30$ is for a fragile behaviour.

The data in Fig. 5 above T_g were fitted with the WLF equation. The obtained parameters were $C_1 = 7.6$ and $C_2 = 59.1\,°C$ with $T_{ref} = 147.5\,°C$ for the DMA results and $C_1 = 9.14$ and $C_2 = 33.0\,°C$ with $T_{ref} = 136.0\,°C$ for creep. However, a deviation from the WLF line is observed at low temperatures, around the glass transition. Below T_g the Arrhenius diagram tends to adopt a linear behaviour, but to see this behaviour in a more clear way data at lower temperature would be necessary. Obviously, the same trend should also be observed in the temperature dependence of the relaxation times, as $\log \tau(T) = \log a_T + \log \tau(T_{ref})$. This behaviour was also found for other authors [36–38], and has also been detected in dielectric relaxation spectroscopy results, although in a much narrow frequency range [39–41].

A theoretical rationalisation of the WLF (or VFTH) equation can be achieved in different ways like, for example, on the basis of the free volume concept [42], or

with the Adam–Gibbs theory [43]. In the later model the temperature dependence of the 'cooperatively rearranging regions' size allows to relate the structural relaxation time with both the temperature and the configurational entropy, S_c

$$\tau(T) = \tau_0 \exp(C/TS_c(T)) \tag{5}$$

where τ_0 and C are constants. S_c can be calculated from the excess heat capacity, $\Delta C_p = C_p(\text{liquid}) - C_p(\text{glass})$

$$S_c(T) = \int_{T_0}^T \frac{\Delta C_p}{T'} dT' \tag{6}$$

where T_0 is the temperature at which S_c extrapolates to zero.

The curvature of $\tau(T)$ in the Ahrrenius diagram comes from the dependence of the configurational entropy with temperature. Different equations for the configurational heat capacity $\Delta C_p(T)$ [26,40]) yield different analytical forms of $S_c(T)$, all of them keeping the characteristic curvature. The glass transition produces a collapse in the conformational mobility and, as a consequence, a smaller temperature dependence of S_c. When a polymer sample is cooled down from equilibrium across the glass transition, the configurational entropy tends to be independent of temperature in the glassy state with a value S_c^g which depends on the cooling rate. This means that in the glassy state, at temperatures below T_g, Eq. (6) takes the Arrhenius equation form with an apparent activation energy $E_a^g = C/S_c^g$. This value is smaller at any temperature than the equilibrium one. The deviation from the equilibrium WLF or Vogel line to the Ahrrenius behaviour implies a decrease in the slope of the log a_T vs. $1/T$ line, as can be seen in Fig. 5.

As seen in Fig. 5, the slope of the log a_T vs. $1/T$ line at temperatures above T_g is higher for the retardation times calculated from creep experiments than for the relaxation times calculated from DMA results. This means that the value of the parameter B in the VFTH equation is not the same for both lines ($B_D = 694.5\,K$ for the compliance and $B_E = 1034.4\,K$ for modulus). On the contrary in poly (propylene glycol) and poly(vinyl acetate) the same temperature dependence of relaxation and retardation times was found [44]. In the case of the PMMA network of this work the difference in slope is high enough to have no doubt of the experimental result. A similar result was found for a PMMA in Ref. [38]. The overlap of the main α relaxation and the secondary β relaxation can be the cause of this peculiar behaviour, in the case of PMMA the β relaxation has been associated with the rotation of the ester group relatively to the C=C bond by which this group is linked to the main chain [45,46] and has an apparent activation energy much smaller than that of the main relaxation [47]. With increasing temperature and frequency the α and β processes approach each other [48] and tend to coalesce originating an unique process called $\alpha\beta$ or a process. Williams [49,50] defined this process as a new relaxation process where the motions associated to the α and β relaxations influence each other and not just a mere superposition

of two relaxation mechanisms. However, the αβ process is not totally clarified, namely it is not so straightforward what happens in the region of frequencies and temperatures where occurs the separation of the two processes (splitting region) [51]. This problem is related to the glass transition dynamics because almost all the details of what the concept cooperativity means are unknown. The αβ process of poly(*n*-alkyl methacrylates) was studied some years ago and several scenarios for the splitting region were proposed not only for these materials but for any material [51]. From this work it is inferred that the behaviour in the splitting region is much more complex than what may be expected, and the way the splitting occurs and the character of the local process could vary considerably in the splitting zone.

Nevertheless, the splitting region in PMMA falls at frequencies much higher than those used in this work, in what β and α relaxation are two independent relaxation process that partially overlap each other. In the frequency dependence of the elastic modulus (Fig. 3) the main relaxation corresponds to the steepest E' step, at the lowest frequencies and for E' values below around $10^{8.5}$ Pa, and the influence of the β relaxation seems to be more important in the high frequency part of the relaxation spectrum. In this frequency range E' increases smoothly with frequency. So, the presence of the secondary relaxation must play an important role in the shifts necessary to superpose the different isotherms to form the master curve.

The situation in the creep compliance $D(t)$, Fig. 4, is similar but now the part of the curve in which the secondary relaxation has the highest influence is that corresponding to the smaller values of D and probably its influence in the global process is smaller. In fact if modulus and compliance were represented in a linear scale against frequency and time, respectively, the former would be representative mainly of the secondary relaxation while the latter would be mainly representative of the α relaxation. The consequence is the difference in the slope of the diagram shown in Fig. 5. The change from VFTH to Ahrrenius appears in both lines at temperatures close to each other as will be discussed below after presenting the TSR results.

3.2. TSR results

Only thermal sampling (TS) experiments are reported in this work, at different T_σ around the glass transition of the studied PMMA. Creep temperatures between 71.5 and 148.5 °C were used. Fig. 6 shows typical results, where the curves are shifted to higher temperatures as T_σ increases and the low temperature plateau presents higher ε values as T_σ increases. This fact was explained elsewhere [22].

Each TS curve contains information about the molecular mobility that mainly occur at the corresponding T_σ for a time scale of about ~ 100 s [24]. The access to the relevant thermo-kinetic parameters of a single TS curve may be achieved by assuming that the response arises from a Debye process. Obviously, this is a simplification as in a real
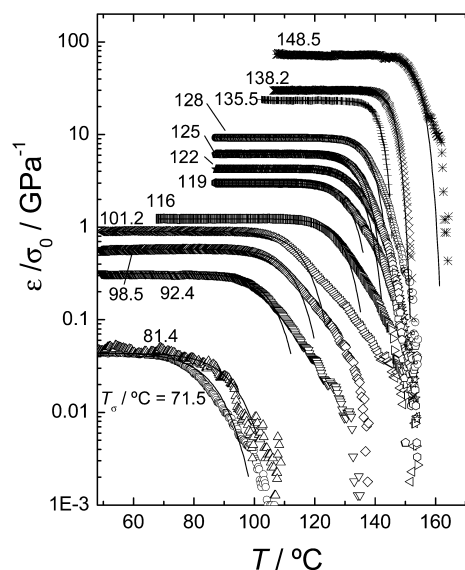

Fig. 6. TS results on the studied PMMA in the glass transition region, obtained at different creep temperatures T_σ (in the graphics). Other experimental conditions: $\beta = 4$ °C min^{-1}, $T_w = 3$ °C, $T_0 = T_\sigma - 50$ °C, $t_\sigma = t_r = 4$ min. The solid lines are the simulated curves with the thermokinetic parameters obtained from the Arrhenius fitting of the $\tau(T)$ results such as those presented in Fig. 7.

situation there is always a distribution of retardation times associated to the relaxational process, that may depend on the TS experimental variables [52]. Assuming an anelastic response described by a Voigt–Kelvin model, the temperature dependence of the retardation time may be given by:

$$\tau(T) = \frac{\varepsilon(T)}{\beta|d\varepsilon(T)/dT|} \tag{7}$$

where $\varepsilon(T)$ is the measured strain as function of temperature and β is the heating rate of the TS experiment.

By numerical derivation of the $\varepsilon(T)$ data, Arrhenius plots may be depicted, using Eq. (7). Using this procedure on the TS data of the studied PMMA some Arrhenius plots are shown in Fig. 7. Assuming an Arrhenius form for $\tau(T)$, due to the short range of τ that are acceded (see data in Fig. 7), the activation energy and the pre-exponential factor may be calculated for each TS curve. More details on the calculation of thermokinetic parameters from TSR data may be found elsewhere [13].

It would be interesting to predict how TSR information could be compatible with usual DMA results, such as the one presented in Section 3.1. Fig. 8 shows a general Arrhenius diagram of an amorphous material near its glass transition. The typical curve of the main characteristic time $\langle\tau\rangle$ is shown, where the WLF behaviour at higher temperature gives rise to an Arrhenius tendency at lower temperatures (below T_g). The thinner lines that envelop the $\langle\tau\rangle$ line pretend to represent a higher and a lower limit for the distribution of characteristic times. Both lines proceed along the reciprocal temperature axis approximately at the same vertical distance from the main $\langle\tau\rangle$ line, as a thermo-rheologically simple system is assumed.
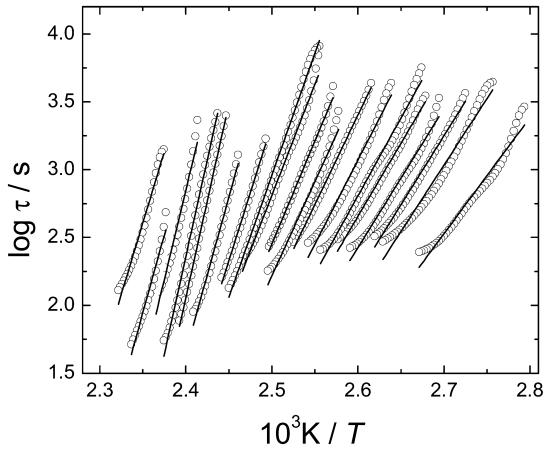
Fig. 7. Arrhenius plot of some TS experiments on the studied PMMA. The solid points were obtained using Eq. (7). The solid lines are the fitting with the Arrhenius equation.

A isothermal dynamic experiment (either a DMA or a dielectric relaxation spectroscopy, DRS, essay) is represented in Fig. 8. The experiment was carried out at $T_{isotherm}$ and D'' or ε'' is plotted against $\log \tau$. A peak is observed with a maximum at about $\tau = \langle \tau(T_{isotherm}) \rangle$. Note that this peak is the result of the relaxation of all the retardation (characteristic) times active at $T_{isotherm}$. TS experiments are also shown in this scheme, as a series of segments that correspond to Arrhenius lines obtained at different T_σ, going from the glassy to the liquid regions. Note that such experiments probe slower molecular motions (higher τ) relatively to typical dynamic experiments, at the same temperature. Moreover, a thinner distribution of characteristic times is monitored, also with respect to isothermal DMA or

dielectric experiments. In fact a TS experiment isolates the retardation times that at T_σ are around τ_σ, as those that are longer are not activated at the creep stage and the shorter ones are relaxed at the isothermal recovery stage, at $T_\sigma - \Delta T_w$. Therefore, as T_σ increases, from the glassy to the liquid state, TS curves are probing narrow distributed molecular motions at a time scale similar to that of a DSC scan (typically ~ 100 s for an heating rate of $10\,^\circ$C min^{-1} [53]), scanning the broad distribution of retardation times in an horizontal way (assuming the scheme of Fig. 8), rather than the vertical scanning of isothermal dynamic tests. The advantage of this horizontal inspection is that it is done in discrete steps: one may find, for example, the apparent activation energy E_a as a function of T_σ for a nearly constant frequency [24]. The scheme of Fig. 8 suggests that in the liquid state the slope of the TS lines (proportional to E_a) should increase as T_σ decreases, i.e. for TS curves going to lower $1/T$ values. However, near T_g, further decrease of T_σ should lead to a decrease of E_a. This was in fact what it was observed, for example, by TSR in a semi-crystalline poly(ethylene terephthalate) [22] and by TSDC in two liquid crystalline polymers [54] and in a series of poly(n-alkyl methacrylates) [55]. Also in the present work the same trend was observed for the studied PMMA, as it is shown in Fig. 9 (circles).

In the case of DMA and creep experiments the apparent activation energy was obtained from the derivative of the experimental shift factor shown in Fig. 5, which should also be similar to the value obtained from the central characteristic time $\langle \tau \rangle$,

$$E_a(T) = R \ln(10) \frac{\mathrm{d} \log a_T}{\mathrm{d}(1/T)} = R \frac{\mathrm{d} \ln\langle \tau \rangle}{\mathrm{d}(1/T)} \qquad (8)$$
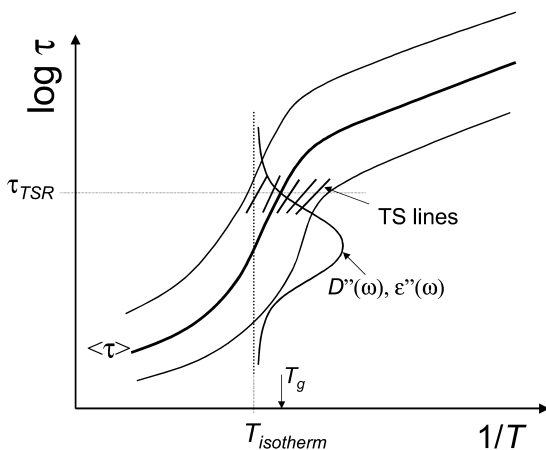

Fig. 8. The main curves are the typical profile of the retardation (characteristic) times in the glass transition region, showing the typical curvature at higher temperature (WLF-like) that tends to an Arrhenius behaviour below T_g. The thicker line is for the mean retardation (characteristic) time ($\langle \tau \rangle$) and the two thinner lines (above and below the main line) represents an envelope of the distribution of characteristic times. The series of segments represents TS lines obtained at different T_σ, that covers a small time-range, around τ_{TSR}. The peak along the $\log \tau$ axis represents schematically an isothermal DMA or dielectric experiment, where D'' or ε'' are plotted against $-\log \omega$, at a temperature $T_{isotherm} > T_g$.
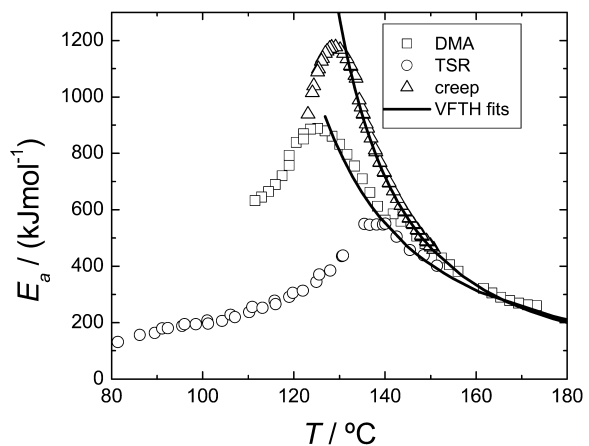

Fig. 9. Temperature dependence of the apparent activation energy across the glass transition of the studied PMMA. The squares are for the DMA results and the triangles are for the creep results, calculated from the temperature shift factors (numerical differentiation). By fitting these shift factors in the liquid state with the WLF equation and using the relations between the WLF and VFTH parameters it was obtained an $E_a(T)$ curve with the corresponding B and T_0 parameters (solid lines). The circles are for the TSR results, where E_a was obtained from the TS curves using Eq. (7) and assuming an Arrhenius behaviour (Fig. 7).

$E_a(T)$ goes through a maximum in the point at which the behaviour start deviating from the equilibrium line. Fig. 9 shows the lines corresponding to DMA and creep results, this kind of plot can be compared with the same representation used for dielectric properties of different polymers [56].

The apparent activation energy can be obtained by TSR at quite low temperatures, far from T_g. This seems to constitute an advantage relatively to both DSC and creep experiments, where the description of the glass transition dynamics could only be performed down to much higher temperatures. In this temperature region (glassy state) E_a depends only slightly on temperature, adopting a characteristic Ahrrenius behaviour. E_a increases with increasing temperatures, going through a maximum when approaching to the VFTH regime, in the equilibrium liquid region at temperatures above T_g. But this approach occurs at temperatures clearly higher than in the case of the characteristic times of the modulus or the compliance. As a consequence the maximum value of E_a is smaller when determined by TSR because in the VFTH regime E_a is a decreasing function of temperature. The reason for this difference comes from the fact that in TSR the measurement is conducted on heating while creep and DMA experiments are isothermal. The behaviour in TSR is analogous to that found in DSC scans conducted on heating after subjecting the sample to a previous thermal treatment that ends at a low temperature, in the glassy state. The heat capacity measured in the heating scan starts with values characteristic of the glassy state $c_{pg}(T)$. The low molecular conformational mobility is responsible for these values of the heat capacity. During heating the glassy response of the material continues until temperatures higher than would be expected from a cooling scan. In other words, the glass transition temperature interval shifts towards higher temperatures in the heating scan with respect to the cooling scan. This shift is highly dependent on the previous thermal history of the sample [57,58]. In the TSR experiments the transition from the Ahrrenius behaviour characteristic of the glass to the VFTH line characteristic of the equilibrium liquid is shifted towards higher temperatures with respect to the data obtained in isothermal experiments. Obviously, such conclusions could be extended to other thermally stimulated techniques such as TSDC.

Above T_g, the E_a values obtained from DMA, creep and TS experiments agree very well. This is due to the fact that, if the system is thermorheologically simple, the slope of $\log\langle\tau\rangle$ vs. $1/T$ (from the DMA data) is similar to the slope of the TS curves in an Arrhenius diagram obtained at the same temperature, although at higher times (see Fig. 8).

3.3. Fragility

As discussed before, fragility is related to the magnitude of the decrease of $\log\tau$ (or $\log a_T$, if one deals with rheological data) with decreasing T_g/T and thus may be parameterised by the steepness 'index' m

$$m = \left.\frac{d\log\tau}{d(T_g/T)}\right|_{T=T_g} = \left.\frac{d\log a_T}{d(T_g/T)}\right|_{T=T_g} \tag{9}$$

The value $m = 16$ corresponds to Arrhenius behaviour (strong limit) and for $m > 200$ the systems reach the fragile limit [9]. The steepness index of many different materials are reported in some works [9,10,59]. Usually polymers appear at the fragile extreme of the Angell plot [9], although one can find also strong polymers [60,61]. It was found that m (that gives the deviation from the Arrhenius behaviour) could be correlated with the non-Debye (or non-exponential) behaviour (often parameterised by the stretched exponential β), for a series of glass-forming liquids [9].

Using Eqs. (3) and (4), m may be directly obtained from the VFTH or WLF parameters. When $T_{ref} = T_g$, m is given by:

$$m = \frac{BT_g/2.303}{(T_g - T_0)^2} = \frac{T_g C_{1g}}{C_{2g}} \tag{10}$$

where C_{1g} and C_{2g} are the coefficients of the WLF equation referred to T_g.

The usual value found for $C_{2g}(\approx 50\,°C)$ indicates that polymers with higher T_g values tend to be the more fragile, which is the case of PMMA (of course there are counter examples).

Note that m may be also obtained directly from the $E_a(T)$ plot, such as the one shown in Fig. 7 (calculated with Eq. (8)) from

$$m = E_a(T_g)/[\ln(10)RT_g] \tag{11}$$

However, fragility has both relaxational and thermodynamic manifestations and m, as defined before, only characterises the relaxational behaviour. In recent works [10,12,62] it is frequent to distinguish between the so-called dynamic or kinetic fragility, measured by m, and the thermodynamic fragility quantified in several ways: usually by the step change on the heat capacity $\Delta C_p(T_g)$ [58] or by the ratio between the absolute heat capacities in the liquid and glassy states (C_p^l/C_p^g) [10], or also by changes on the coefficient of thermal expansion [63] or on the excess entropy [64]. In all cases these variations are calculated at T_g.

As suggested by the Adam–Gibbs theory kinetically fragile liquids are expected to have large configurational heat capacities, resulting from their configurational entropy changing rapidly with temperature and kinetically strong liquids are expected to have small configurational heat capacities. For small molecule glasses this statement seems to be valid [2,65,66] but for polymers this is not so straightforward [11,61,67]. There are several works where it is shown that thermodynamic and kinetic fragilities are not strongly correlated [11,68] especially for polymeric systems. This means that a kinetically fragile system is not necessarily a thermodynamically fragile system.

DSC can be used to study kinetic fragility. In this case the apparent activation energy around T_g, usually called Δh^* [53,60], may be obtained from the variation of the fictive temperature with the cooling rate, q_c, in DSC scans according to Refs. [53,69]

$$\frac{d \ln q_c}{d(1/T'_f)} = -\frac{\Delta h^*}{R} \quad (12)$$

T'_f is the limit value of the fictive temperature defined as the temperature corresponding to the point of intersection of enthalpy curves of the glassy and the liquid states [70]. Similarly to Eq. (11) the fragility index may be calculated with $m = \Delta h^*/[\ln(10)RT_g]$.

Different DSC traces obtained at $10\,°C\,min^{-1}$, after different cooling rates (between 0.5 and $40\,°C\,min^{-1}$) are shown in Fig. 10. The $\ln q_c$ vs. $1/T'_f$ plot of the studied PMMA is shown in Fig. 11. From the slope of the corresponding linear fitting we found $\Delta h^* = 771.6\,kJ\,mol^{-1}$ that leads to $m = 102$, a value which is similar to the one reported in literature ($m = 103$) for PMMA [71] also determined by DSC. It should be noticed that the use of DSC in the determination of m may lead to great errors, especially in fragile materials, where the variation of T'_f with q_c is less pronounced, introducing significant inaccuracy in Δh^* determination.

DSC was also used to evaluate the thermodynamic fragility and in this case we use the step change on the heat capacity ΔC_p at T_g. A value of $\Delta C_p(T_g) = 0.21\,Jg^{-1}\,k^{-1}$ was obtained which is similar with the value found in literature for a PMMA: $\Delta C_p(T_g) = 0.25\,Jg^{-1}\,k^{-1}$ [72], although the obtained value is somewhat smaller as expected for a slightly crosslinked material. Comparing this value of ΔC_p with values found for other systems [62,72], this PMMA can be classified as a thermodynamically strong system. This classification in agreement with the one found in Ref [10] for PMMA, although they used the (C^l_p/C^g_p) criterion. Angell suggested that this strong behaviour in polymers arises from the influence of chain
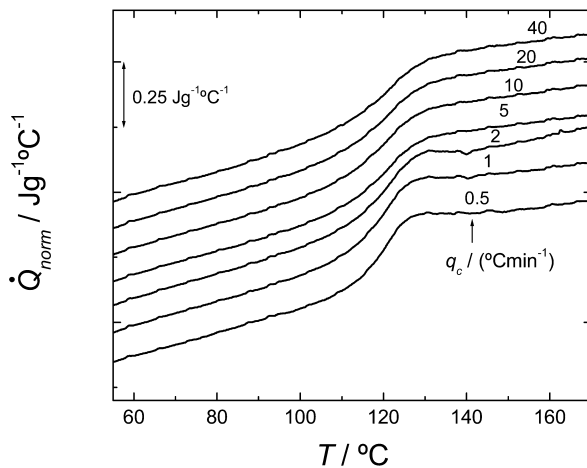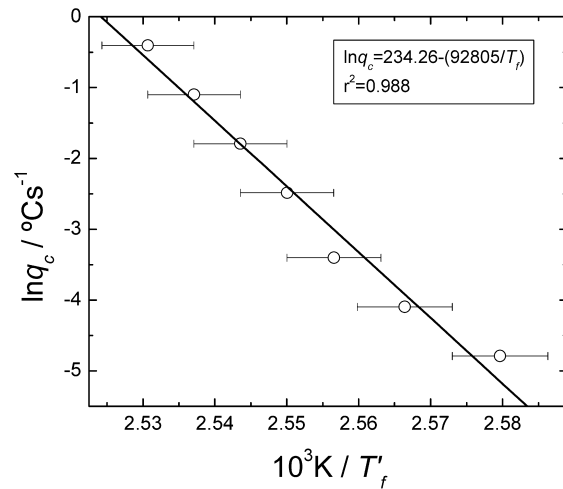

Fig. 11. logarithm of cooling rate ($\ln q_c$) versus the reciprocal of limit fictive temperature ($1/T'_f$) with the corresponding linear fitting, that allowed to calculate $\Delta h^* = 771.6\,kJ\,mol^{-1}$.

length or entanglements [73] and that these two effects move T_g to higher temperatures resulting in a smaller C^l_p/C^g_p than the one predicted. From this point of view polymers should have a greater dynamic fragility than other materials and a smaller thermodynamic fragility. It is interesting to see how in Ref. [72] the authors observe for several systems the large values of $\Delta C_p(T_g)$ for the smaller m. However, as noted in Ref. [10] this explanation does not provide a complete picture of this behaviour since there are examples of polymers that fall in all the possible combinations of kinetic–thermodynamic fragility [10]. As noted by the authors this matter needs further investigation.

The high temperature dependence of the apparent activation energy in the VFTH equation makes the fragility parameter m highly dependent of the criterion used to determine T_g. It is usual to define T_g according to some *ad hoc* criterion, most of the times the temperature for which the relaxation time is 100 s. However, the differences between the relaxation times measured by different techniques makes non-sense a comparison of the absolute values of the fragility parameters determined with different techniques. The clear example is the difference between the viscoelastic relaxation and retardation times. The great difference between D_R and D_U makes τ_D and τ_E to be several decades in time apart from each other. From our results it can be estimated that the temperature at which τ_D is 100 s is 15° higher than that at which τ_E is 100 s. A possible another criterion for T_g, which was chosen in this work, is the maximum of the $E_a(T)$ curve. With this assumption the DMA results would yield a value of $T_g(DMA) = 125\,°C$ and using Eq. (11) $m \approx 117$ while creep experiments yield $T_g(creep) = 128\,°C$ and $m \approx 153$. A value of $m \approx 145$ was found by mechanical spectroscopy for PMMA in reference [10]. So, according to the fragility scale the PMMA network can be classified as a kinetically fragile system with a not Arrhenius transport behaviour. As expected for fragile

Fig. 10. DSC traces obtained for the studied PMMA at $10\,°C\,min^{-1}$ after cooling from the liquid state at different rates $q_c = dT/dt$ (in the graphics).

systems the apparent activation energy is high, usually fragile systems have E_a of 500 kJ mol^{-1} or more near T_g (in our case E_a is even higher), corresponding to a change in dynamics of one decade for a temperature change of 3–5 K [3].

As explained above the maximum of the $E_a(T)$ curve corresponding to the TSR technique is shifted towards higher temperatures and lower E_a values with respect to DMA and creep techniques are obtained, this obviously leads to a lower value of the fragility parameter ($m \approx 70$). It is interesting to note that the maximum value of E_a obtained by TSR in this work is similar to the ones found in literature for PMMA by thermally stimulated creep(≈ 590 kJ mol^{-1}) [74] and TSDC (≈ 350 kJ mol^{-1}) [75].

Also in other polymers lower values of $E_a(T_g)$ were obtained using thermally stimulated methods comparatively to the ones corresponding to other techniques (DSC, DMA, creep). For example, for polycarbonate and from TSDC results $E_a(T_g) \approx 317$ kJ mol^{-1} [76] and as $T_g \approx 158$ °C (defined by the same criterion used in this work) m will be ≈ 40, but by mechanical spectroscopy $m \approx 132$ [9] which implies a much higher $E_a(T_g)$ value. For amorphous PET and from TSDC results $E_a(T_g) \approx 457$ kJ mol^{-1} [76] and $T_g \approx 69$ °C that will lead to a $m \approx 70$, but by DSC a value of $m \approx 156$ was obtained [10]. So the lower values of m obtained by TSR (and TSDC) comparatively to the ones obtained by other techniques for the same material seem to be a consequence of the particular thermal profile of this technique.

4. Conclusions

In the case of the PMMA network studied in this work, DMA (E' and tan δ) and creep compliance master curves were successfully obtained by simple shifting. For these techniques the shift factors above T_g were well described by the WLF equation: Below T_g a deviation from the Vogel behaviour was observed and the Arrhenius diagram adopted a linear behaviour. The change from the Vogel to an Arrhenius behaviour was explained by the temperature dependence of the configurational entropy.

From the log a_T vs. $1/T$ representation it was clearly seen that at temperatures above T_g the temperature dependence of the retardation times calculated from creep results and the temperature dependence of the relaxation times calculated from DMA results was not the same. This behaviour is the opposite of what is found in other materials and was attributed to the superposition of the α and β relaxations of PMMA. We supposed that the influence of the β relaxation would be distinct for the creep compliance and elastic modulus curves, being smaller in the case of the creep compliance curve; this would lead to a distinct temperature dependence of the retardation and the relaxation times.

From TSR it was possible to obtain the apparent activation energy at low temperatures far from T_g, an information not easily available from DMA or creep techniques. In this temperature range E_a depends only slightly on temperature, which is consistent with a nearly overall Arrhenius behaviour for the mean characteristic times in the glassy state. As the TSR experiments were conducted on heating while DMA and creep were isothermal, the change from an Arrhenius to a Vogel behaviour was detected at higher temperatures for TSR and the associated maximum E_a value was lower. Above T_g the E_a values obtained from DMA, creep and TSR experiments agreed very well.

Finally, the fragility of this PMMA network was also investigated. It should be pointed that the fragility index, m, is highly dependent on the criterion used to determine T_g. In our case T_g was defined as the temperature of the maximum of the $E_a(T)$ curve. From DMA $m = 117$ and from creep $m = 153$. m was also calculated from DSC results and a value of $m = 103$ was obtained. So according to these results the PMMA network could be classified as kinetically fragile system. These values are in agreement with the ones found in literature for PMMA. By TSR lower values of m would be obtained due to the particular thermal profile of this technique as explained before. DSC was also used to evaluate the thermodynamic fragility and in this case we adopted the criterion of the step change on the heat capacity ΔC_p at T_g. A value of $\Delta C_p(T_g) = 0.21$ Jg^{-1} k^{-1} was obtained. Comparing this value with the values found for other systems in literature we classified this PMMA network as a thermodynamically strong system.

References

[1] Stillinger FH. Science 1995;267:1935.
[2] Angel CA. Science 1995;267:1924.
[3] Ediger MD, Angel CA, Nagel SR. J Phys Chem 1996;100:13200.
[4] Ngai KL. J Non-Cryst Solids 2000;275:7.
[5] Angell CA. J Non-Cryst Solids 1991;131–133:13.
[6] Oldekop VW. Glasstechnische Berichte 1957;30:8.
[7] Laughlin WT, Uhlmann DR. J Phys Chem 1972;76:2317.
[8] Plazek DJ, Ngai KL. Macromolecules 1991;24:1222.
[9] Böhmer R, Ngai KL, Angell CA, Plazek DJ. J Chem Phys 1993;99: 4201.
[10] Huang D, McKenna GB. J Chem Phys 2001;114:5621.
[11] Ngai KL, Roland CM. Macromolecules 1993;26:6824.
[12] Green JL, Ito K, Xu K, Angell CA. J Phys Chem B 1999;103:3991.
[13] Alves NM, Mano JF, Gómez Ribelles JL. J Therm Anal Calorim 2002;70:633.

[14] Lacabanne C, Chatain D, Monpagens JC. J Macromol Sci Phys 1977; B134:537.

[15] Monpagens JC, Lacabanne C, Chatain D, Hiltner A, Baer A. J Macromol Sci Phys 1978;B15:503.

[16] Lacabanne C, Chatain D, Monpagens JC, Berticat P. J Appl Phys 1979;50:2723.

[17] Van Turnhout J. Polym J 1971;2:173.

[18] Van Turnhout J. Thermally stimulated discharge of polymer electrets. Amsterdam: Elsevier; 1975.

[19] Alves NM, Mano JF, Gómez Ribelles JL. Macromol Symp 1999;148: 437.

[20] Alves NM, Mano JF, Gómez Ribelles JL. Polymer 2001;42:4173.

[21] Alves NM, Mano JF, Gómez Ribelles JL. Mater Res Innovat 2001;4: 170.

[22] Alves NM, Mano JF, Gómez Ribelles JL. Polymer 2002;43:3627.

[23] Cuesta Arenas JM, Mano JF, Gómez Ribelles JL. J Non-Cryst Solids 2002;307–310:758.

[24] Mano JF. Thermochim Acta 1999;332:161.

[25] Correia NT, Alvarez C, Moura Ramos JJ. Polymer 2000;41:8625.

[26] Correia NT, Alvarez C, Moura Ramos JJ, Descamps M. J Chem Phys 2000;113:3204.

[27] Ferry JD. Viscoelastic properties of polymers, 3rd ed. New York: Wiley; 1980.

[28] Ngai KL, Plazek DJ. Rubber Chem Tech Rubber Rev 1995;68:376.

[29] Ngai KL, Plazek DJ, Rendell RW. Rheol Acta 1997;36:307.

[30] Plazek DJ, Chay IC, Ngai KL, Roland CM. Macromolecules 1995;28: 6432.

[31] Pethrick RA, Davis WJ. Polymer 1998;39:255.

[32] Williams ML, Landel RF, Ferry JD. J Am Ceram Soc 1953;77:3701.

[33] Vogel H. Phys Z 1921;22:645.

[34] Fulcher GA. J Am Chem Soc 1925;8:339.

[35] Tamman G, Hesse WZ. Anorg Allg Chem 1926;156:245.

[36] Hideshima TJ. Jpn Soc Test Mater 1961;10:246.

[37] Hideshima T. In: Seitz, Turnbull D, editors. Solid physics, vol. 14. New York: Academic Press; 1963.

[38] Higgenbotham-Bertolucci PR, Gao H, Harmon JP. Polym Engng Sci 2001;41:873.

[39] Alegria A, Guerrica-Echevarría E, Goitiandía L, Tellería I, Colmenero J. Macromolecules 1995;28:1516.

[40] Saito S. J Appl Polym Sci 1959;2:93.

[41] Schlosser E. Polym Bull 1982;8:461.

[42] Doolittle AK. J Appl Phys 1951;22:1471. Doolittle AK. J Appl Phys 1952;23:236.

[43] Adams G, Gibbs JH. J Chem Phys 1958;43:139.

[44] Ngai KL, Mashimo S, Fytas G. Macromolecules 1988;21:3030.

[45] Heijboer J. Proc Int Congr Phys Non-Cryst Sol, Delft 1964;.

[46] Muzeau E, Perez J, Johari GP. Macromolecules 1991;24:4713.

[47] McCrum NG, Read BE, Williams G. Anelastic and dielectric effects in polymeric solids. New York: Dover; 1967.

[48] Williams G. Adv Polym Sci 1979;33:59.

[49] Williams G. Trans Faraday Soc 1966;62:2091.

[50] Williams G, Watts DC. In: Karasz FE, editor. Dielectric properties of polymers. New York: Plenum Press; 1972.

[51] Garwe F, Schönhals A, Lockwenz H, Beiner M, Schröter K, Donth E. Macromolecules 1996;29:247.

[52] Alves NM, Mano JF, Gómez Ribelles JJ. Polym Int 2002;51:434.

[53] Moynihan CT, Easteal AJ, deBolt MA, Tucker J. J Am Ceram Soc 1976;59:12.

[54] Moura Ramos JJ, Mano JF, Coates D. Mol Cryst Liq Cryst 1996;281: 267.

[55] Dudognon E, Bernes A, Lacabanne C. Polymer 2002;43:5175.

[56] Gómez Ribelles JL, Diaz Calleja R. Anales de Fisica, Serie B 1985; 81:104.

[57] Berens AR, Hodge IM. Macromolecules 1982;15:756.

[58] Berens AR, Hodge IM. Macromolecules 1985;18:1980.

[59] Rössler E, Hess KU, Novikov VN. J Non-Cryst Solids 1998;223:207.

[60] Roland CM. Macromolecules 1992;25:7031.

[61] Santangelo PG, Ngai KL, Roland CM. Macromolecules 1996;29: 3651.

[62] Saiter A, Devallencourt C, Saiter JM, Grenet J. Eur Polym J 2001;37: 1083.

[63] Colluci DM, Mckenna GB, Filliben JJ, Lee A, Curliss DB, Bowman KB, Russel JD. J Polym Sci, Polym Phys Ed 1997;35:1561.

[64] Ito K, Moynihan CT, Angell CA. Nature 1999;398:493.

[65] Ngai KL, Plazek DJ. Rubber Chem Technol 1995;68:376.

[66] Angell CA, Richards BE, Velikov V. J Phys: Condens Matter 1999; 11:A75.

[67] Roland CM, Santangelo PG, Ngai KL. J Chem Phys 1999;111:5593.

[68] Johari GP. J Chem Phys 2000;112:8958.

[69] Litovitz TA. J Chem Phys 1952;20:1088.

[70] Tool AQ. J Am Ceram Soc 1946;29:240.

[71] Donth E. J Polym Sci, Phys Ed 1996;34:2881.

[72] Hempel E, Hempel G, Hensel A, Schick C, Donth E. J Phys Chem B 2000;104:2460.

[73] Angell CA. In: Tant MR, Hill AJ, editors. Structure and properties of glassy polymers. Washington, DC: American Chemical Society; 1998. p. 37–52.

[74] Doulut S, Demont P, Lacabanne C. Macromolecules 2000;33:3425.

[75] Sauer BB, Avakian P. Polymer 1992;33:5128.

[76] Bernes A, Chatain D, Lacabanne C. Polymer 1992;33:4682.